

Energy-Efficient Transmission Range and Duration for Cognitive Radio Sensor Networks

Mustafa Ozger, Ecehan B. Pehlivanoglu, and Ozgur B. Akan, *Fellow, IEEE*

Abstract—Cognitive Radio (CR) promises an efficient utilization of radio spectrum resources by enabling dynamic spectrum access to overcome the spectrum scarcity problem. Cognitive Radio Sensor Networks (CRSNs) are one type of Wireless Sensor Networks (WSNs) equipped with CR capabilities. CRSN nodes need to operate energy-efficiently to extend network lifetime due to their limited battery capacity. In this paper, for the first time in literature, we formulate the problem of finding a common energy-efficient transmission range and transmission duration for all CRSN nodes and network deployment that would minimize the energy consumed per goodput per meter toward the sink in a greedy forwarding scenario. Results reveal non-trivial relations for energy-efficient CRSN transmission range and duration as a function of nine critical network parameters such as primary user activity levels. These relations provide valuable insights for detailed CRSN designs prior to deployment.

Index Terms—cognitive radio, sensor networks, hop progress, energy-efficiency, transmission range, transmission duration, goodput.

I. INTRODUCTION

The proliferation of wireless devices has caused spectrum scarcity since the available spectrum is not efficiently utilized with the current fixed spectrum allocation approach. Dynamic Spectrum Access (DSA) is a paradigm to overcome such inefficiencies, by allowing unlicensed users to leverage the idle licensed spectrum. Cognitive Radio (CR) has been proposed as the key enabling technology for the realization of DSA. CR is applied to Wireless Sensor Networks (WSNs) to form Cognitive Radio Sensor Networks (CRSNs), making the most use of available spectrum for sensor networks without the burden of spectrum licensing costs [1].

Given the energy constraints of unlicensed CRSN nodes, called Secondary Users (SUs), communication between a CRSN source node and the remote sink takes place through multiple hops under DSA. Successful frame transmission under DSA in each hop depends on certain requirements. Firstly, SU transmitter and receiver nodes need to be in the transmission range of each other (i.e., they need to be topologically connected one-hop neighbors), and both need to correctly identify the same portion of the spectrum as idle

M. Ozger is with the School of Electrical Engineering and Computer Science, KTH Royal Institute of Technology, Stockholm, Sweden. e-mail: ozger@kth.se.

E. B. Pehlivanoglu and O. B. Akan are with Next-generation and Wireless Communications Laboratory (NWCL), the Department of Electrical and Electronics Engineering, Koc University, Istanbul, 34450, Turkey. e-mail: epehlivanoglu@ku.edu.tr.

O. B. Akan is also with Internet of Everything (IoE) Group, Electrical Engineering Division, Department of Engineering, University of Cambridge, CB3 0FA Cambridge, UK. e-mail: oba21@cam.ac.uk.

through spectrum sensing. Secondly, a licensed user, called Primary User (PU), should not arrive on that portion of the spectrum during the SU transmission. In case of a PU arrival, the SU pair need to restart sensing the spectrum in the next time slot and attempt retransmission if they can seize some portion of the spectrum. In this context, transmission range and duration have a non-trivial impact on the energy-efficient operations of a CRSN. A larger transmission range results in a fewer number of hops toward the remote sink yet faces higher energy consumption at each hop and a bigger potential number of PUs that may interrupt the SU communications. On the other hand, a smaller transmission range decreases energy consumption at each hop and reduces the number of interfering PUs but increases the number of hops to reach the remote sink, hence might potentially increase overall source-to-sink energy consumption. Additionally, a longer transmission duration can deliver more bits in one transmission slot for a given bit rate, yet is more susceptible to incoming PUs on the accessed part of the spectrum during transmission.

Transmission range is often a set parameter before sensor network deployment as simple sensor nodes may not have complex power control capabilities [2], [3]. Furthermore, power control may not be cost-effective under DSA due to limited energy-saving potential and added protocol complexity [4]. Energy-efficient transmission range is even more important in the CRSN context, given its impact on successful frame transmission under DSA schemes limited battery capacity. Existing works that shed light on transmission range for ad hoc wireless networks and WSNs prior to their deployment [5], [6] are not directly applicable to the CRSN context given the intermittent nature of communication under DSA. Furthermore, there is no study dedicated to finding transmission range and duration for all nodes in CRSN as design parameters. Additionally, while it could be possible for CRSN to tune its transmission duration, finding an energy-efficient duration for different scenarios prior to deployment is key. In fact, [13] considers this from the perspective of energy-efficient packet size. To that end, energy-efficient transmission range and duration can be studied with a composite metric on energy consumed per goodput per meter progress toward the sink at each hop.

Recent research on CRSNs focused mostly on spectrum sensing [7], [8], [9], spectrum decision and handoff [10], [11], clustering [12], physical layer studies on adaptive modulation [14], CR-enabled Internet of Things [15] and channel bonding for CRSN [16] and attempts on MAC layer [17], network layer [18] and transport layer [19] protocols and solutions. In addition, full-duplex communication with non-orthogonal

multiple access is also investigated for security and reliability of in CR-enabled networks [20], [21]. Also, the authors in [22] focus on maximization of minimum data rate in IoT networks with energy harvesting and CR capabilities. Although these studies are important to realize CRSNs, there is clearly a need to study homogeneous energy-efficient transmission range and duration for CRSN nodes. Since the sensors are simple devices with limited computational and battery capacities, changing transmission range and duration under the dynamic spectrum access environment would be prohibitive. Hence, our analysis serves as valuable guidelines for designers on how to set a fixed transmission range and duration prior to the deployment.

In this paper, for the first time in literature, we formulate the problem of finding energy-efficient homogeneous transmission range and duration for the nodes in CRSN deployments. To that end, we define two clear objectives, which then translate into the network model and consequent analyses to shed light on energy-efficient transmission range and duration for CRSNs:

- **Objective 1: Spectrum-aware transmissions:** Transmission range and duration should enable efficient transmission in each hop. The success of frame transmission on each hop of a CRSN depends on (i) Presence of a spectrum opportunity and its correct sensing (after false alarms and mis-detections are accounted for) both by the transmitter and the receiver; (ii) No PU arrival during the entire transmission duration on the accessed spectrum portion; (iii) Correct reception of all bits on the receiver side under the unreliable radio link model.
- **Objective 2: Energy-efficient operations:** Transmission range and duration should ensure overall energy-efficiency of the CRSN. This depends on the minimization of energy consumed per goodput per meter progress toward sink at each hop, hence increasing overall network energy-efficiency.

Contributions of our paper are as follows. Following these two core objectives, we first clearly lay our non-binding assumptions on the system model. Secondly, we characterize the transmissions in CRSN under DSA; deriving the probability of successful frame transmission at each attempt between one-hop neighbor CRSN nodes, extending the study in [23]. Thirdly, we derive expected hop progress from the source toward the sink at each hop (i.e. meters taken toward the sink at each hop). Given a homogeneous transmission range, we lay out the expected hop progress (i.e. the expected progress toward the sink at each hop) as well as the expected hop distance (i.e. the expected distance between one-hop neighbors) in a greedy forwarding scheme. From the expected hop distance, we reveal the expected energy consumption until successful frame transmission under different spectrum utilization scenario probabilities. Finally, we derive the energy consumed per goodput per-hop progress in meter toward the sink and reveal optimal transmission range and transmission duration values thereof. The main contribution of this paper is to reveal energy-efficient homogeneous transmission range and transmission duration for CRSN deployment and to investigate its relationship with the following critical network parameters:

path loss exponent (κ), PU death and birth rates (α and β), PU node density (ρ_p), Radius of PU guarding protection zone (r_p), Reference Signal-to-Noise Ratio (SNR) at SU receivers for correct demodulation (γ_0), Power consumed by SU during spectrum sensing (P_s), Maximum SU-PU collision probability that a PU can tolerate (P_{col}), Ratio of PU signal variance (σ_p^2) to noise variance (σ_n^2).

The remainder of the paper is organized as follows. In Section II, the system model to investigate the energy-efficient transmission range and duration for CRSN is introduced. Derivations related to DSA characteristics, energy consumption dynamics of each node, successful frame transmission probability under the DSA scheme, and energy consumption thereof are presented in Section III. For a given homogeneous transmission range, we study the expected hop progress toward the sink as well as expected hop distance in a greedy forwarding scheme in Section IV. Using this result, we derive the non-closed form equation for energy-efficient homogeneous transmission range and duration for CRSN in the same section. The numerical results are presented and discussed in Section V, and the paper is concluded in Section VI.

II. SYSTEM MODEL

In our system model, there are two types of network devices. The PUs have exclusive access to the licensed spectrum. On the other hand, the SUs access these licensed bands opportunistically, i.e., whenever there are no PU transmissions on them. The following features are incorporated in our analysis:

- PUs coexist with SUs on a 2-dimensional circular area (called \mathcal{F} , of radius Γ).
- Both PUs and SUs are randomly deployed over \mathcal{F} with 2-D homogeneous Poisson Point Processes (PPP) with means ρ_p and ρ_s , respectively.
- CRSN has a flat structure. Each SU node senses its environment and transmits event information to the sink in multiple hops. The sink resides at the center of \mathcal{F} .
- Simple greedy forwarding is assumed as routing mechanism [25]. Hence, an SU's next hop neighbor to transmit its field sensing information is assumed to be the neighbor within a range of r_s that is closest to the remote sink.
- SU nodes are assumed to know their neighbors' locations with respect to the remote sink, through a geographical location service [26].
- SUs have a common predetermined channel list, which they follow during periodic spectrum sensing operations [24]. This list may be provided by a centralized spectrum sharing mechanism. Formation of the optimal channel list is beyond the scope of this paper, and its effect on our analysis is neutralized assuming all channels have the same PU density, PU activity model and bandwidth.
- Time is slotted for SU-SU communication. In each slot, two one-hop neighbors that are willing to communicate sense a licensed channel from their channel list, for Spectrum Access (SA). If they run out of channels in their list, they restart in a circular fashion.
- Two SU neighbors have a Spectrum Opportunity (SO) if i) they are not within the guarding of any PU at all

times OR ii) the PUs in whose guardring they reside are all inactive during spectrum sensing. The guardring of a PU is centered at that PU's location, with radius r_p .

- Spectrum sensing might be erroneous. In case both SUs correctly sense the SO, that event is called Successful Spectrum Access (SSA).
- In case any of the two SU neighbors sense (either correctly or erroneously) a PU presence during spectrum sensing on the licensed channel, they perform spectrum handoff, moving to the next channel in their channel list, in a circular fashion.
- When two SU neighbors carry out SA (whether successful or not), *Frame Transmission (FT)* is started. In case no PU arrives during frame transmission, Successful Frame Transmission (SFT) takes place. Otherwise, the SU packet is not correctly delivered, and both SUs perform spectrum handoff to the next channel at the end of the transmission. We assume there is no dedicated radio to notify the SUs that a PU has arrived on the channel they communicate [24], hence in such a case SUs perform spectrum handoff at the end of the transmission slot τ_f .
- The PU activity is modeled as exponentially distributed inter-arrivals, with a two state birth-death process with death rate α and birth rate β . As a result of this birth-death process, the licensed spectrum portion under scrutiny can have ON and OFF states. An ON (Busy) state represents the period where this spectrum portion is occupied by PUs, whereas an OFF (Idle) state represents the period where it is unused. The length of the ON and OFF periods are exponentially distributed [13], [27].

III. ANALYSIS FRAMEWORK

A. Spectrum Sensing Events and Their Probabilities

The time is slotted, with two periods in each slot. The first period is reserved for spectrum sensing (τ_s), and the subsequent period is for the frame transmission (τ_t). Total duration of one slot is $\tau_f = \tau_s + \tau_t$, as depicted in Fig. 1.

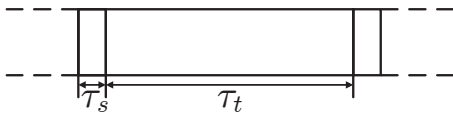


Fig. 1: The time slot structure.

T_{idle} and T_{busy} are the random variables that define the idle and busy time periods of each licensed channel with probability distribution functions $f_{T_{idle}}(t) = \beta e^{-t\beta}$ and $f_{T_{busy}}(t) = \alpha e^{-t\alpha}$, as per PU activity model explained in Section II [27]. Resultant channel probabilities are $P_{idle} = \alpha/(\alpha + \beta)$ and $P_{busy} = \beta/(\alpha + \beta)$, respectively.

Due to its practicality, energy detection based spectrum sensing is assumed, with non-zero false alarm and mis-detection probabilities. Let the hypotheses \mathcal{H}_0 and \mathcal{H}_1 define idle and busy channel conditions, respectively. Hence, the probability of false alarm is

$$P_{fa} = Pr[Busy, \mathcal{H}_0] = P_{idle} \mathcal{Q}\left(\frac{\delta - 2\tau_s B \sigma_n^2}{\sqrt{4\tau_s B \sigma_n^4}}\right), \quad (1)$$

where B is the bandwidth of the channel, δ is the detection threshold, σ_n^2 is the noise variance, and $\mathcal{Q}(\cdot)$ is Q-function [27]. The probability of correct busy detection is given as

$$P_d = Pr[Busy, \mathcal{H}_1] = P_{busy} \mathcal{Q}\left(\frac{\delta - 2\tau_s B (\sigma_p^2 + \sigma_n^2)}{\sqrt{4\tau_s B (\sigma_p^2 + \sigma_n^2)^2}}\right), \quad (2)$$

where σ_p^2 is the PU signal variance [27]. Probabilities of correct detection of idle spectrum and mis-detection are given as follows, respectively:

$$P_v = P_{idle} - P_{fa}, \quad (3)$$

$$P_{md} = P_{busy} - P_d. \quad (4)$$

B. Energy Consumption Dynamics

Energy consumed in each hop has three components. The first component is E_s , consumed for spectrum sensing during τ_s at the beginning of each slot. Both the transmitter SU and the receiver SU in a one-hop transmission consume $E_s = P_s \tau_s$ amount of energy for each spectrum sensing operation.

The second component is E_t , energy consumed for transmission which is a function of r_s and τ_t , and can be formulated as [6], [28]

$$E_t = (q_1 r_s^\kappa + q_2) \tau_t, \quad (5)$$

where κ is the path loss exponent, r_s is the transmission range and τ_t is the transmission period in a single time slot. q_1 and q_2 can be defined as [6]

$$q_1 = \frac{\gamma_0 N_{rx} N_0 B (\frac{4\pi}{\lambda})^\kappa 10^\kappa}{G_a \eta_{amp}}, \quad (6)$$

$$q_2 = P_{elec}, \quad (7)$$

where γ_0 is the minimum required signal-to-noise (SNR) ratio at the receiver's demodulator, N_{rx} is the noise figure of the receiver, N_0 is the thermal noise in a 1 Hz bandwidth, B is the channel bandwidth, λ is the signal wavelength, η_{amp} is the transmitter amplifier efficiency, G_a is the antenna gain and P_{elec} is the power consumed by the device.

The third component is E_r , energy consumed on receiver side, formulated as $E_r = P_{rx} \tau_t$, where P_{rx} is the receiver power consumption.

C. Spectrum Utilization Scenarios

The spectrum holes are utilized opportunistically by SUs. Without loss of generality, MAC level scheduling between SUs is assumed to be collision-free, which can be enabled for a communicating SU pair via Guaranteed Time Slots through MAC layer protocols such as IEEE 802.15.4 [29]. Additionally, as mentioned in Section II, a central entity or cluster heads can ensure SUs receive customized licensed channel lists for access.

For a successful transmission to take place among two one-hop neighbors, four conditions need to be met in total:

- The first two conditions are on finding a Spectrum Opportunity (SO) through reliable spectrum sensing on both

TABLE I: Scenarios for utilization of spectrum opportunities in the system model, probabilities and energy consumption thereof.

		Spectrum Access (SA)				Frame Transmission (FT)					
		TX sensing		RX sensing		PU arrival in τ_t		Reliability in τ_t			
S #	Init. state	Event	Prob.	Event	Prob.	Event	Prob.	Event	Prob.	Total probability	Cons. energy
S1	P_{idle}	FA ¹	$\overline{P_{fa}}$	FA ¹	$\overline{P_{fa}}$	-	1	-	1	$P_{idle} \overline{P_{fa}}^2$	$2E_s$
S2	P_{idle}	FA ¹	$\overline{P_{fa}}$	CVD ²	$\overline{P_v}$	-	1	-	1	$P_{idle} \overline{P_{fa}} \overline{P_v}$	$2E_s$
S3	P_{idle}	CVD ²	$\overline{P_v}$	FA ¹	$\overline{P_{fa}}$	-	1	-	1	$P_{idle} \overline{P_{fa}} \overline{P_v}$	$2E_s$
S4	P_{idle}	CVD ²	$\overline{P_v}$	CVD ²	$\overline{P_v}$	≥ 1 PU ⁵	$1 - P_{np}$	-	1	$P_{idle} \overline{P_v}^2 (1 - P_{np})$	$2E_s + E_t + E_r$
S5	P_{idle}	CVD ²	$\overline{P_v}$	CVD ²	$\overline{P_v}$	No PU	P_{np}	≥ 1 , error	$1 - P_r$	$P_{idle} \overline{P_v}^2 P_{np} (1 - P_r)$	$2E_s + E_t + E_r$
S6	P_{idle}	CVD ²	$\overline{P_v}$	CVD ²	$\overline{P_v}$	No PU	P_{np}	No error	P_r	$P_{idle} \overline{P_v}^2 P_{np} P_r$	$2E_s + E_t + E_r$
S7	P_{busy}	CBD ³	$\overline{P_d}$	CBD ³	$\overline{P_d}$	-	1	-	1	$P_{busy} \overline{P_d}^2$	$2E_s$
S8	P_{busy}	CBD ³	$\overline{P_d}$	MD ⁴	$\overline{P_{md}}$	-	1	-	1	$P_{busy} \overline{P_d} \overline{P_{md}}$	$2E_s$
S9	P_{busy}	MD ⁴	$\overline{P_{md}}$	CBD ³	$\overline{P_d}$	-	1	-	1	$P_{busy} \overline{P_d} \overline{P_{md}}$	$2E_s$
S10	P_{busy}	MD ⁴	$\overline{P_{md}}$	MD ⁴	$\overline{P_{md}}$	-	1	-	1	$P_{busy} \overline{P_{md}}^2$	$2E_s + E_t + E_r$

¹False Alarm || ²Correct Vacant Detection || ³Correct Busy Detection || ⁴Mis-Detection || ⁵At least 1 PU arrives within duration τ_t

the transmitter and the receiver sides, and are referred to as conditions for Successful Spectrum Access (SSA).

- The second two conditions cover the cases that throughout the transmission of the frame in τ_t , no PUs arrive on the channel and no bit errors occur on the transmitted frame, and referred to as conditions for Successful Frame Transmission (SFT).

Different events in these four conditions bring about 10 scenarios in total, which are summarized in Table I. Within notations from Table I, it should be noted that $\overline{P_{fa}} = P_{fa}/P_{idle}$, $\overline{P_v} = P_v/P_{idle} = (P_{idle} - P_{fa})/P_{idle}$, $\overline{P_d} = P_d/P_{busy}$ and $\overline{P_{md}} = P_{md}/P_{busy} = (P_{busy} - P_d)/P_{busy}$.

In the scenarios S1-S6 from Table I, the licensed channel (that the SU transmitter SU_{TX} and receiver SU_{RX} are both sensing) is idle during spectrum sensing, presenting an SO. In this context, the SU_{TX} and SU_{RX} could correctly sense this channel as idle and access it subsequently. However, given imperfections in energy detection based spectrum sensing, there might be cases where they decide not to access this channel despite it being idle, summarized as scenarios S1-S3. These 3 scenarios cover the cases that at least one of the SU_{TX} and SU_{RX} decide the channel is busy, despite the SO, referred to as a False Alarm (FA) case. Consequently, SSA does not take place in scenarios S1-S3, and total energy consumed by the SU_{TX} and SU_{RX} is $2E_s$, for spectrum sensing operations.

In scenarios S4-S6, the SU_{TX} and SU_{RX} correctly identify the SO and achieve SSA. What differs in between these 3 cases are the fulfillment of two conditions for SFT. First condition is regarding the potential arrival of PU(s) during a time interval of τ_t on the channel that the SU_{TX} and SU_{RX} previously accessed. Any potential PU in the shaded area around the SU_{TX} and SU_{RX} illustrated in Fig. 2 should remain silent during τ_t so that no PU-SU collision occurs. With the underlying assumption that PU transmission range r_p is greater than SU transmission range r_s , no PU arrival

probability during τ_t is expressed as

$$P_{np} = \sum_{k=0}^{\infty} \frac{e^{-\rho_p S} (\rho_p S)^k}{k!} (e^{-\tau_t \beta})^k = e^{-\rho_p S} \left(\sum_{k=0}^{\infty} \frac{(\rho_p S e^{-\tau_t \beta})^k}{k!} \right) = e^{-\rho_p S (1 - e^{-\tau_t \beta})}, \quad (8)$$

where the first term in (8) is the probability of having k PUs in the area S illustrated in Fig. 2 according to Poisson distribution, and the second term is the probability that all of these k PUs remain silent at least for a duration of τ_t as per the PU activity model from Section II. The area S between the SU_{TX} and SU_{RX} that are z apart can be defined as

$$S(z, r_p) = 2\pi r_p^2 - 2r_p \cos^{-1} \left(\frac{z}{2r_p} \right) + \frac{z}{2} \sqrt{4r_p^2 - z^2}. \quad (9)$$

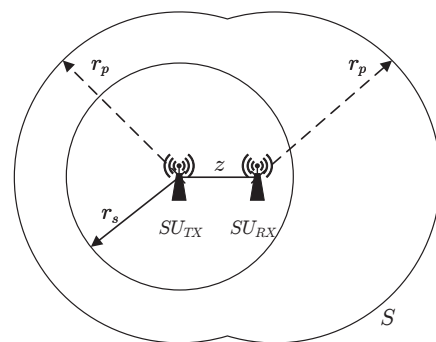


Fig. 2: Illustration of guarding concept.

The second condition to achieve SFT once SSA is achieved is that all bits of the transmitted frame are received correctly on SU_{RX} side. Under unreliable radio link model [31], the probability that all the bits in the frame are received successfully can be written as

$$P_{rel} = (1 - BER(\gamma))^{\zeta}, \quad (10)$$

TABLE II: Probability mass function of random variable T .

Number of trials (t)	$P(T = t)$
1	P_C
2	$P_C(P_A + P_B)$
3	$P_C(P_A^2 + 2P_A P_B + P_B^2)$
4	$P_C(P_A^3 + 3P_A^2 P_B + 3P_A P_B^2 + P_B^3)$
...	...

where BER is the bit error rate (BER) to evaluate the unreliability of the link, γ is the signal-to-noise ratio in the receiver, $\zeta = \tau_t R = \tau_t B \log_2(1 + \gamma)$ is the packet size sent during τ_t in bits with theoretically achievable rate R . The BER can be written as $BER(\gamma) = 0.5 \operatorname{erfc}(\sqrt{k}\gamma)$ where $\operatorname{erfc}(x) = \frac{2}{\sqrt{\pi}} \int_{\sqrt{x}}^{\infty} \exp(-u^2) du$ is the complementary error function [30]. The channel is assumed to be an AWGN channel, and k depends on the modulation type used. If the modulation type is BPSK, then $k = 1$.

Under these conditions, as can be followed from Table I, only scenario S6 refers to SSA followed by SFT. The probability of this scenario can be calculated as follows:

$$\begin{aligned} P_{S6} &= P_v^2 P_{np} P_{rel} \\ &= (P_{idle} - P_{fa})^2 (e^{-\rho_p S(1-e^{-\tau_t B})}) (1 - BER(\gamma))^{\zeta} \end{aligned} \quad (11)$$

In scenarios S7-S10, the sensed licensed channel is busy when the SU_{TX} and SU_{RX} start their spectrum sensing, hence there is no SO available. In scenarios S7-S9, at least one of the SU_{TX} and SU_{RX} correctly detects this channel as busy. Consequently, both nodes carry out spectrum handoff to the next channel in their list and total energy consumed by them in that slot is $2E_s$, for spectrum sensing operations. However, in scenario S10, the SU_{TX} and SU_{RX} both incorrectly sense the channel as idle, which in turn triggers the SU frame transmission that will not result in an SFT. The probability of this scenario is

$$P_{S10} = P_{md}^2 = \left(P_{busy} \mathcal{Q} \left(\frac{2\tau_s B(\sigma_p^2 + \sigma_n^2) - \delta}{\sqrt{4\tau_s B(\sigma_p^2 + \sigma_n^2)^2}} \right) \right)^2, \quad (12)$$

where P_{md} is the mis-detection probability by an SU. Total energy consumed in that slot for S10 is $2E_s + E_t + E_r$, as SU_{TX} and SU_{RX} try to communicate, despite no SO being available, due to double mis-detection on both sides.

From a joint SFT and energy consumption perspective, there are three sets of scenarios:

- Set A : $\{S1, S2, S3, S7, S8, S9\}$, consisting of scenarios with no SFT and an energy consumption of $2E_s$ only.
- Set B : $\{S4, S5, S10\}$, consisting of scenarios with no SFT and an energy consumption of $2E_s + E_t + E_r$ due to failed transmission.
- Set C : $\{S6\}$, consisting of the only scenario with SFT and an energy consumption of $2E_s + E_t + E_r$.

As part of finding an energy-efficient transmission range r_s and transmission duration τ_t for SUs, it is of interest to compute the expected energy consumption among an SU_{TX} and SU_{RX} that are z apart. We are specifically interested in

the probability mass function (PMF) for the random variable T that denotes number of time slot trials until event C (i.e. scenario S6) resulting in an SFT takes place. Let us denote the probabilities of three independent events A, B, C as P_A, P_B, P_C respectively. Then the probability mass function for the random variable T , which represents the number of trials until SFT is achieved, can be illustrated as in Table II and expressed as:

$$P(T = t) = \sum_{k=0}^{t-1} P_C \left(\binom{t-1}{k} P_A^k P_B^{t-1-k} \right). \quad (13)$$

The expected energy consumption until SFT between SU_{TX} and SU_{RX} that are z apart is

$$\begin{aligned} E\{E_{sft}\} &= \sum_{t=1}^{\infty} \sum_{k=0}^{t-1} P_C \left(\binom{t-1}{k} P_A^k P_B^{t-1-k} \right) \\ &\quad \times (E_C + kE_A + (t-1-k)E_B), \end{aligned} \quad (14)$$

where $E_A = 2E_s$ and $E_B = E_C = 2E_s + E_t + E_r$. Similarly, expected time until SFT is

$$\begin{aligned} E\{\tau_{sft}\} &= \sum_{t=1}^{\infty} \sum_{k=0}^{t-1} P_C \left(\binom{t-1}{k} P_A^k P_B^{t-1-k} \right) \\ &\quad \times ((t-k)(\tau_s + \tau_t) + k\tau_s). \end{aligned} \quad (15)$$

IV. ENERGY-EFFICIENT r_s AND τ_t FOR CRSN

Our aim is to lay the foundations to investigate energy-efficient homogeneous transmission range r_s and transmissions duration τ_t numerically for CRSNs in Section V. To that end, we first revisit the strong foundations on expected hop progress, denoted as $E\{W\}$, from the source toward sink at each hop [5]. The assumed routing approach is a greedy forwarding scheme called Least Remaining Distance (LRD), which would guarantee to minimize the remaining distance to the sink at each hop. Secondly, based on expected hop progress toward the sink, we derive the expected hop distance $E\{Z\}$ under the LRD scheme. Using $E\{Z\}$, the expected energy consumption, i.e., $E\{E_{sft}\}$ and time until SFT, i.e., $E\{\tau_{sft}\}$, can be computed using scenario probabilities as in (14-15). We later use $E\{W\}$, $E\{Z\}$ and $E\{E_{sft}\}$ to numerically compute optimal homogeneous transmission range r_s^* and transmission duration τ_t^* in Section V.

A. Expected Hop Progress

To study the expected hop progress toward the sink at each hop, we consider the setup illustrated in Fig. 3. Let SU_{TX} be the CRSN node with relevant information that needs to be conveyed to the sink. SU_{TX} has a transmission radius of r_s and would need to trigger multi-hopping toward the sink, unless $r_s < X$, in which case a single hop would suffice. SU_{TX} employs the LRD as the greedy forwarding scheme, choosing its neighbor in the forwarding region that is closest to the sink as the next hop and attempts SSA and SFT subsequently. The forwarding region for SU_{TX} is defined by $A_F = A_{F1} \cup A_{F2}$.

Given DSA and successful communication probabilities derived in detail in Section III-C, SU_{TX} continues its attempts

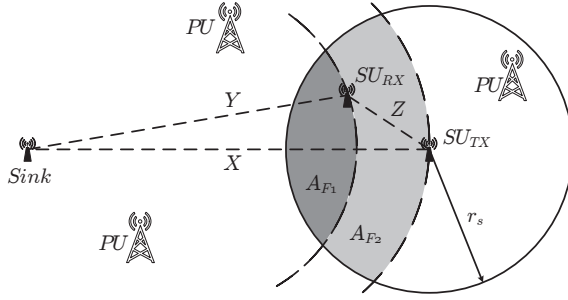


Fig. 3: Illustration of forwarding approach.

until SFT is achieved. At each hop, the same process is repeated, hence, each hop can be regarded as the first step of the remaining forwarding process toward the sink [4], [5].

For the setup in Fig. 3, assume that SU_{TX} chooses node SU_{RX} as its next hop neighbor according to LRD greedy forwarding [25]. Per system model characteristics, both SU and PU locations are assumed to be random. Therefore, all the distances between SU_{TX} , SU_{RX} and the sink can be characterized by random variables. Let the distances between SU_{TX} and the sink, SU_{RX} and the sink and SU_{TX} and SU_{RX} be represented by the random variables X , Y and Z , respectively. In this context, $W = X - Y$ is the random variable that represents hop progress. LRD forwarding chooses the neighbor of SU_{TX} in the region $A_F = A_{F1} \cup A_{F2}$ with minimum Y , which in turn maximizes W . In the example in Fig. 3, this neighbor is SU_{RX} , with no other neighbor closer to the sink being present in the region A_{F1} .

W also depends on the distance between SU_{TX} and the sink. When $X \leq r_s$, SU_{TX} and the sink are one-hop neighbors, the hop progress is then automatically equal to X . If $X > r_s$, there must be a neighbor node in the forwarding region for hop progress toward the sink. This condition can be represented by the following random variable:

$$F = \begin{cases} 1 & \text{, if there is a neighbor in the forwarding region,} \\ 0 & \text{, otherwise.} \end{cases} \quad (16)$$

The expected hop progress is described and calculated as in (19), which is studied in detail in [5]. Since CRSNs have usually high and even ultra-high densities, the following approximations,

$$1 - e^{-\rho_s A_{F1}} \approx 1 \text{ and } 1 - e^{-\rho_s A_F} \approx 1, \quad (17)$$

can be made. Then, $E\{W\}$ expression simplifies to

$$E\{W\} = r_s - \frac{r_s^3}{3\Gamma^2}. \quad (18)$$

B. Expected Hop Distance

Although $r_p > r_s$ is strictly assumed, it is also considered that transmission ranges of PUs and SUs are comparable, so that channel availability for SUs has both spatial and temporal variations, as in our previous work [23]. Hence, SO depends on the distance between SU_{TX} and SU_{RX} . This distance, depicted as Z in Fig. 4, determines the area of the guarding (as per (9)) where there should be no active PU for a duration of τ_t after SSA. To that end, Z has a direct impact on the expected energy $E\{E_{sft}\}$ and time $E\{\tau_{sft}\}$ required to achieve SFT.

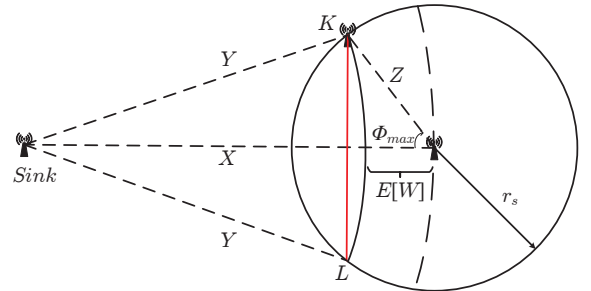


Fig. 4: Relation between hop progress and hop distance.

For a given $E\{W\} = w$, the next hop node SU_{RX} can be uniformly anywhere on the black solid arc that is from point K to point L as seen in Fig. 4. We assume linear approximation for the KL arc to decrease the computational burden, which is shown by the solid red line in Fig. 4. With this approximation, the angle Φ between the edges that are X and Z long is uniformly distributed in $[-\Phi_{max}, \Phi_{max}]$. With the aforementioned approximation, for a given $E\{W\} = w$, it is clear that $\Phi_{max} = \cos^{-1}(\frac{E\{W\}}{r_s}) = \cos^{-1}(\frac{w}{r_s})$. Additionally, the hop distance can be written as $Z = \frac{w}{\cos(\Phi)}$ for a random point on the red line, with its maximum being equal to r_s . The expected hop distance for a given $E\{W\} = w$ is then

$$\begin{aligned} E\{Z|w\} &= \int_{-\Phi_{max}}^{\Phi_{max}} \frac{w}{2\Phi_{max} \cos(\Phi)} d\Phi, \\ &= \frac{w}{2\Phi_{max}} \left(\ln(\tan(\Phi_{max}) + \sec(\Phi_{max})) \right. \\ &\quad \left. - \ln(\tan(-\Phi_{max}) + \sec(-\Phi_{max})) \right). \end{aligned} \quad (20)$$

The expected value given in (20) is evaluated and plugged into (9) to calculate guarding sizes for different network scenarios in Section V.

$$\begin{aligned} E\{W|((X \leq r_s) \cup (X > r_s \cap F = 1))\} &= \int_0^\infty \Pr\{W > w|((X \leq r_s) \cup (X > r_s \cap F = 1))\} dw \\ &= \frac{3\Gamma^2 r_s - 6 \int_0^{r_s} \int_{r_s}^\Gamma x e^{-\rho_s A_{F1}} dx dw}{3(x^2 - 2 \int_{r_s}^\Gamma x e^{-\rho_s A_F} dx)} \end{aligned} \quad (19)$$

C. Energy-Efficient Transmission Range and Duration

Based on the derivations for SSA and SFT probabilities from Section III-C and study of expected hop progress toward the sink and hop distance in a greedy forwarding scheme from Sections IV-A and IV-B, we are ready to formulate the optimization problem. The optimization aims to find (r_s^*, τ_t^*) pair that would maximize the goodput-meter per Joule achieved in the provided CRSN system model. Hence, the optimization problem can be formulated as a reward function Λ as

$$\begin{aligned} \max_{r_s, \tau_s} \quad & \Lambda = \frac{\tau_t R}{\frac{E\{\tau_{sft}\}}{E\{E_{sft}\}}} \cdot E\{W\} \\ \text{subject to} \quad & 0 < r_s < r_p, \\ & 0 < \tau_t < \tau_{max}, \end{aligned} \quad (21)$$

where the unit for Λ is (bits/s) \times m per Joule. The maximum transmission duration constraint, τ_{max} , is

$$\tau_{max} = -\frac{1}{\mu} \log \left(1 - \frac{P_{col}}{P_{idle}} \right) \quad (22)$$

where $\mu = \max\{\alpha, \beta\}$ and P_{col} is the maximum SU-PU collision probability that a PU can tolerate [27]. Thanks to our approximation in (17), (21) becomes an optimization problem with a quadratic objective function with linear constraints.

V. NUMERICAL RESULTS

In this section, first of all, we provide the preliminaries on required spectrum sensing duration τ_s given the desired transmission duration τ_t and the maximum SU-PU collision probability that a PU can tolerate P_{col} [27]. Consequently, behavior of the SFT probability P_{S6} as the underlying driver of the reward function Λ given in (21), is studied for different (r_s, τ_t) scenarios. Moving forward, the reward function Λ is evaluated and examined in detail. As part of that, sensitivities of optimal $(r_s^*, \tau_t^*, \Lambda^*)$ values with respect to changes in 9 critical network parameters are tabulated in detail. As a last step, how optimal $(r_s^*, \tau_t^*, \Lambda^*)$ values respond to combined changes in path loss exponent κ , PU death rate α and birth rate β are examined. Employed parameters and their values throughout all following analyses, unless otherwise stated, are provided in Table III.

A. Preliminaries on τ_t and τ_s

Transmission duration τ_t is one of the two decision variables (r_s, τ_t) for the reward function Λ in (21) that is intended to be maximized. Sensing duration τ_s also directly affects SFT probability P_{S6} in a slot for the given system model, yet cannot be chosen arbitrarily. In fact, τ_s is dependent on the desired τ_t value, driven by the maximum SU-PU collision probability that a PU can tolerate P_{col} , hence is not a decision variable in our problem formulation.

For the optimization purposes in this paper, τ_s - τ_t relation from [27] has been adopted. More specifically, for given α , β , τ_t and P_{col} values, the maximum value of the false alarm probability allowed as per P_{col} requirement is

$$P_{fa} = P_{idle} P_{busy} - P_{idle} P_{busy} \left(1 - \frac{P_{col}}{P_{idle}} \right) e^{\mu \tau_t} \quad (23)$$

TABLE III: Parameters and their assumed values from [5], [6], [27].

Parameter	Symbol	Value
PU birth rate	β	3 / s
PU death rate	α	3 / s
PU guardring radius	r_p	200 m
Path loss exponent	κ	2.5
Reference SU SNR	γ_0	20 dB
PU signal vs. noise variance	$\gamma_p = \sigma_p^2 / \sigma_n^2$	10
Receiver noise figure	F_{rx}	12.589
Thermal noise	N_0	4.17×10^{-21} W/Hz
Bandwidth	B	10 kHz
Signal wavelength	λ	0.125 m
Amplifier efficiency	η_{amp}	0.2
Antenna gain	G_a	0.01
TX circuit power consumption	P_{elec}	3.63 mW
Spectrum sensing power cons.	P_s	700 mW
RX total power consumption	P_{rx}	11.13 mW
Network diameter	Γ	1000 m

and τ_s is picked such that mis-detection and false alarm probabilities are equal, i.e. $P_{fa} = P_{md}$. This serves to balance interference caused upon PUs through mis-detection and lost spectrum opportunities through false alarm. With this approach, τ_s is given by

$$\tau_s = \frac{1}{B\gamma_p^2} \left(Q^{-1} \left(\frac{P_{fa}}{P_{idle}} \right) + (\gamma_p + 1) Q^{-1} \left(\frac{P_{fa}}{P_{busy}} \right) \right)^2. \quad (24)$$

Required τ_s for different P_{col} constraints are depicted in Fig. 5(a). Inherently, required τ_s that satisfies $P_{fa} = P_{md}$ is prolonged as P_{col} constraint gets stricter. Additionally, with higher P_{col} , slope of the τ_t vs. τ_s increases.

As per this τ_s - τ_t relation, it is of interest to reveal how much of the spectrum is intended and used for communications across time. Two metrics can be employed for that purpose. First one is the spectrum efficiency, defined as the intended ratio for communications in a slot, i.e. $\Theta = \frac{\tau_s}{\tau_s + \tau_t}$ [27]. Second one is the SFT efficiency, defined as the ratio of time used for communications to actual time spent until SFT is achieved, i.e. $\Omega = \frac{\tau_t}{E\{\tau_{sft}\}}$. Fig. 5(b) illustrates both metrics for different P_{col} cases. As seen in Fig. 5(b), Θ monotonically increases in the given τ_t interval, whereas Ω peaks around 0.6-0.8 msec interval, depending on the case for P_{col} . Although neither Θ nor Ω considers energy efficiency, Ω provides a better indication for likely optimal τ_t^* values for the problem here, given the $(\tau_t R) / E\{\tau_{sft}\}$ term in (21). Optimal τ_t values from Ω perspective, i.e. $\tau_t^{*,\Omega}$, for $P_{col} = 0.07$ is $\tau_t^{*,\Omega} = 0.63$ msec, for $P_{col} = 0.04$ is $\tau_t^{*,\Omega} = 0.72$ msec and for $P_{col} = 0.01$ is $\tau_t^{*,\Omega} = 0.78$ msec. As stricter P_{col} constraints drive τ_s significantly, it is logical that $\tau_t^{*,\Omega}$ follows this upward trend.

Consequently, in the following analyses, SFT efficiency Ω and suitable values for τ_s - τ_t thereof will be considered to optimize the reward function in (21).

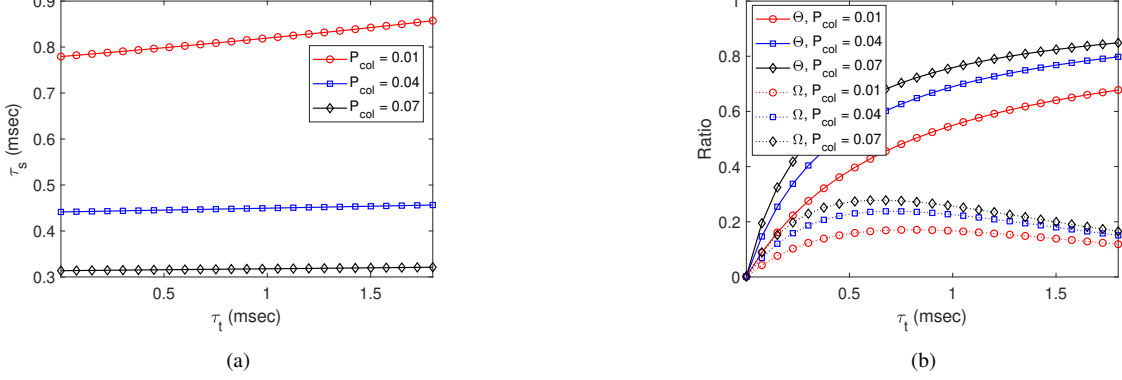


Fig. 5: (a) Required spectrum sensing duration τ_s vs. τ_t for different P_{col} cases; (b) Comparison of sensing efficiency (defined as $\Theta = \frac{\tau_s}{\tau_s + \tau_t}$) and SFT efficiency (defined as $\Omega = \frac{\tau_t}{E\{\tau_{sft}\}}$) [24] for different P_{col} cases.

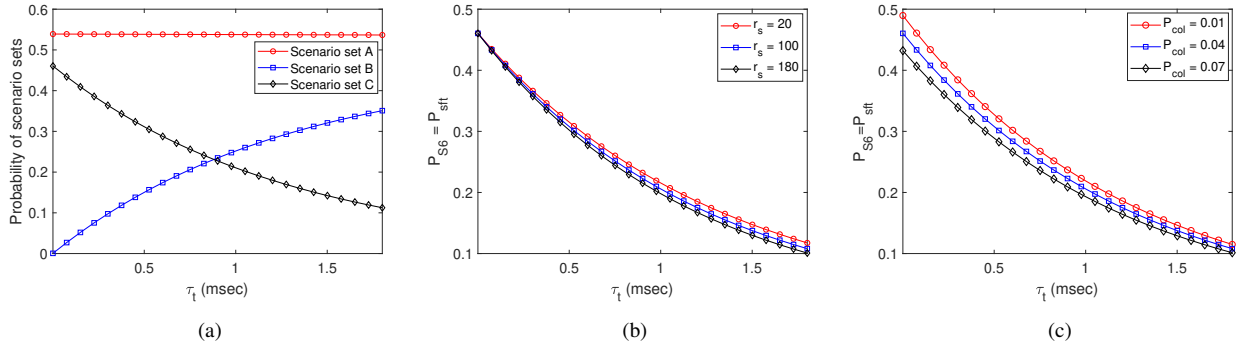


Fig. 6: (a) Probabilities of scenario sets A, B and C vs. τ_t ; (b) Probability of success scenario P_{S6} vs. τ_t for different r_s cases; (c) Probability of success scenario P_{S6} vs. τ_t for different P_{col} cases.

B. Behavior of SFT probability P_{S6}

As part of the optimization process of the reward function Λ in (21), it is important to reveal how the probability of SFT, i.e. P_{S6} behaves and varies with critical parameters. Fig. 6(a) depicts the probabilities of scenario sets A, B and C (which were previously defined in Section III-C) with respect to τ_t , using parameter values defined in Table III. Accordingly, the probability of set A, which includes scenarios related to no SSA and is denoted by P_A , is relatively flat with changing τ_t . This result is natural, given the fact that P_A includes two types of events:

- Sensed channel is idle, yet at least one of the SU TX and RX sense the channel as occupied.
- Sensed channel is busy, and at least one of the SU TX and RX sense the channel as occupied.

The probabilities of both of these event types depend on spectrum sensing duration τ_s , which is also relatively flat with changing τ_t , as previously illustrated in Fig. 5(a). On the other hand, the probability of SFT, i.e. $P_C = P_{S6}$ decays quickly toward null with increasing τ_t . To that end, P_{S6} and hence reward function Λ in (21) are significantly sensitive to changes in τ_t .

Fig. 6(b) breaks-down the same P_{S6} further by different r_s cases with respect to τ_t . Consequently, the effect of varying r_s on P_{S6} is insignificant when τ_t is low, yet suddenly becomes material with increasing τ_t . In fact, increasing r_s from 20 m

to 180 m reduces P_{S6} only by 1% when $\tau_t = 0.5$ msec; yet same r_s change reduces P_{S6} by 14% when $\tau_t = 1.8$ msec. To that end, effect of r_s and τ_t changes on P_{S6} are correlated and requires further deep-dive.

Fig. 6(c) details the combined effect of P_{col} and τ_t on P_{S6} . A stricter P_{col} requirement brings a lower $P_{fa} = P_{md}$, hence SFT probability P_{S6} is higher for $P_{col} = 0.01$ compared to when $P_{col} = 0.07$ as in Fig. 6(c). P_{S6} reduces by $\sim 10\%$ as P_{col} is relaxed from 0.01 to 0.07, with very little variation as τ_t is increased. To that end, effect of P_{col} and τ_t changes on P_{S6} are uncorrelated. Additionally, although a stricter P_{col} brings a higher P_{S6} in each slot, it still results in a lower SFT efficiency Ω as previously revealed in Fig. 5(b).

C. Reward Function Λ With Respect to r_s and τ_t

After the preliminary on τ_s - τ_t relation, and how P_{S6} reacts to changes in τ_s , τ_t and P_{col} ; it is time to construct the reward function Λ . Fig. 7 provides a sample illustration of Λ for the parameter values given in Table III. The reward function Λ is smooth and well defined for all $r_s < r_p$ and $\tau_t < \tau_{max}$, as seen in Fig. 7. For this sample illustration, optimal $(r_s^*, \tau_t^*, \Lambda^*)$ trio is $(40$ m, 0.1 msec, 6.8×10^7 (bps \times m)/Joule). We examine in detail how $(r_s^*, \tau_t^*, \Lambda^*)$ trio responds to changes in critical network parameters in Section V-D.

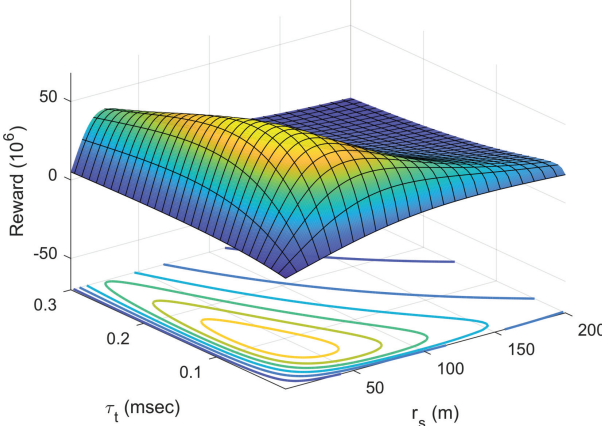


Fig. 7: Illustration of the reward function for values in Table III.

TABLE IV: Changes to terms of the reward function Λ in (21) when only individual parameters are increased.

Event	$E\{\tau_{sft}\}$	$E\{E_{sft}\}$	$E\{W\}$	R
$\kappa \uparrow$	\leftrightarrow	\uparrow	\leftrightarrow	\downarrow
$\beta \uparrow$	\uparrow	\uparrow	\leftrightarrow	\leftrightarrow
$\alpha \uparrow$	\downarrow	\downarrow	\leftrightarrow	\leftrightarrow
$\rho_p \uparrow$	\uparrow	\uparrow	\leftrightarrow	\leftrightarrow
$r_p \uparrow$	\uparrow	\uparrow	\leftrightarrow	\leftrightarrow
$\gamma_0 \uparrow$	\leftrightarrow	\uparrow	\leftrightarrow	\uparrow
$P_s \uparrow$	\leftrightarrow	\uparrow	\leftrightarrow	\leftrightarrow
$P_{col} \uparrow$	\downarrow	\downarrow	\leftrightarrow	\leftrightarrow
$\sigma_p^2/\sigma_n^2 \uparrow$	\downarrow	\downarrow	\leftrightarrow	\leftrightarrow

\uparrow : Increases || \downarrow : Decreases || \leftrightarrow : No change observed

D. Sensitivity of Optimal r_s^* , τ_t^* and Λ^*

Assuming parameter base values and (r_s^*, τ_t^*) are kept, Table IV reveals how individual changes in parameters, all else being equal, impact each term on the reward function Λ^* .

On the other hand, Table V presents the sensitivity of optimal $(r_s^*, \tau_t^*, \Lambda^*)$ to individual changes in 9 critical network parameters, ceteris paribus. The base values for each parameter, from which the sensitivities are tested, are provided in second column of Table V. Third and fourth columns together indicate how sensitive optimal $(r_s^*, \tau_t^*, \Lambda^*)$ trio are to changes in the corresponding network parameter. Next paragraphs detail out the impact of each parameter on network design and provides the reasoning thereof.

1) *Sensitivity to κ :* Path loss exponent κ is the parameter that optimal $(r_s^*, \tau_t^*, \Lambda^*)$ are most sensitive to. When κ is raised, all else being equal (incl. base value (r_s^*, τ_t^*)), $E\{E_{sft}\}$ increases and achievable rate R decreases, as shown in Table IV. Increase in $E\{E_{sft}\}$ is very significant, driven by the fact that consumed energy in transmission is $E_t = (q_1 r_s^\kappa + q_2) \tau_t$. To that end, it is clear that new optimal Λ^* that to be attained once (r_s^*, τ_t^*) are updated will be much lower.

Given the E_t equation form, to arrive at the new optimal Λ^* , shift in r_s^* in the reverse direction of the change in κ is more effective compared to a change in τ_t^* . Hence, r_s^* moves significantly in the reverse direction of the κ change. Albeit not at the order of r_s^* , τ_t^* also shifts significantly with changes in κ . However, in contrast to r_s^* , τ_t^* moves in the same direction as κ , as indicated in rows 1-3 of Table V.

2) *Sensitivity to β :* PU birth rate β is the second parameter that optimal Λ^* is most sensitive to. All else being equal (incl. base value (r_s^*, τ_t^*)), a rise in β increases both $E\{\tau_{sft}\}$ and $E\{E_{sft}\}$, as given in Table IV. This is driven by the fact that a surge in β drives down both P_{idle} probability for SSA as well as P_{np} probability for SFT once SSA is achieved.

Adjustments on (r_s, τ_t) have little to no impact on P_{idle} and P_{fa} probabilities that drive the likelihood of SSA. However, both decision variables are directly relevant for $P_{np} = e^{-\rho_p S(1-e^{-\tau_t \beta})}$, which is the relevant probability to complete SFT after SSA is achieved. To optimize the reward function, system chooses to increase $E\{W\}$ via increasing r_s and reduce chances for PU arrival during frame transmission by decreasing τ_t , as indicated in rows 4-6 of Table V. Consequently, both r_s^* and τ_t^* shift respectably as a response to changes in β . r_s^* moves in the same direction as β , while τ_t^* shifts to the reverse. It is worth noting that an increase in r_s^* is possible here, despite an increase in β , driven by the low base value for PU node density ρ_p .

3) *Sensitivity to α :* PU death rate α is the third parameter that optimal reward is most sensitive to. When α rises, both $E\{\tau_{sft}\}$ and $E\{E_{sft}\}$ decrease, as revealed in Table IV. This is driven by the fact that a surge in α boosts P_{idle} hence likelihood of SSA.

To arrive at new optimal Λ^* , since average idle time of each channel is distributed exponentially with mean $1/\beta$, there is no reason for τ_t to increase as α increases. On the other hand, an increase in α surges P_{idle} to help SSA, yet has no impact on P_{np} that is relevant for SFT after SSA is achieved. Therefore, optimization seeks to maximize $P_{np} = e^{-\rho_p S(1-e^{-\tau_t \beta})}$, which is the probability that no PU arrives to the channel during frame transmission. It is much easier to raise this probability by decreasing τ_t rather than r_s , as S is a slowly increasing function with respect to r_s . To that end, all else being equal, τ_t^* and r_s^* are negatively correlated with α , with τ_t^* having a much higher sensitivity, as in rows 7-9 of Table V.

4) *Sensitivity to ρ_p :* Optimal $(r_s^*, \tau_t^*, \Lambda^*)$ are slightly sensitive to changes in PU node density ρ_p . All else being equal (incl. base value (r_s^*, τ_t^*)) when ρ_p is increased, both $E\{\tau_{sft}\}$ and $E\{E_{sft}\}$ rise, as tabulated in Table IV. This in turn decreases the attainable Λ value.

Parameter ρ_p essentially has no direct link to likelihood of SSA, yet is impacting $P_{np} = e^{-\rho_p S(1-e^{-\tau_t \beta})}$ and hence SFT probability through the S term, which is defined as $S(w, r_p) = 2\pi r_p^2 - 2r_p \cos^{-1}(\frac{w}{2r_p}) + \frac{w}{2} \sqrt{4r_p^2 - w^2}$. Here, $E\{W\} = w$ for a given r_s . As shown in rows 10-12 of Table V, when r_p is changed, to arrive at new optimal Λ^* , τ_t^* is mildly shifted in the opposite direction while r_s^* is slightly moved in the same direction. In that sense, as ρ_p rises, system chooses progressing more meters toward the sink at each hop at the expense of reduced transmission time. It should be noted that an increase in r_s^* is possible here, despite an increase in ρ_p , driven by the low base value for ρ_p .

5) *Sensitivity to r_p :* Optimal $(r_s^*, \tau_t^*, \Lambda^*)$ are slightly sensitive to changes in PU guarding radius r_p . All else being equal (incl. base value (r_s^*, τ_t^*)) when r_p is increased, both $E\{\tau_{sft}\}$ and $E\{E_{sft}\}$ rise, as in Table IV. It is clear that

TABLE V: Sensitivity of optimal r_s^* , τ_t^* and Λ^* values with respect to changes in critical network parameters.

Parameter	Base value	Variable	Sensitivity	Change in decision variables and reward when parameter is changed by...								
				-50%	-25%	-10%	-5%	+5%	+10%	+25%	+50%	
κ	2.5	r_s^*	●	—	—	+242%	+74%	-42%	-63%	-88%	-97%	
		τ_t^*	●	—	—	-11%	-5%	+5%	+9%	+17%	+32%	
		Λ^*	●	—	—	+199%	+64%	-39%	-59%	-86%	-96%	
β	3.0	r_s^*	○	-14%	-7%	-3%	-1%	+1%	+3%	+7%	+15%	
		τ_t^*	○	+9%	+5%	+2%	+1%	-1%	-2%	-5%	-10%	
		Λ^*	●	+59%	+25%	+9%	+4%	-4%	-8%	-19%	-34%	
α	3.0	r_s^*	○	+9%	+3%	+1%	+1%	—	-1%	-2%	-3%	
		τ_t^*	●	+25%	+9%	+3%	+1%	-1%	-3%	-6%	-11%	
		Λ^*	●	-43%	-19%	-7%	-3%	+3%	+6%	+14%	+25%	
ρ_p	0.001	r_s^*	○	-5%	-5%	-2%	-1%	+1%	+2%	+4%	+8%	
		τ_t^*	○	+15%	+14%	+5%	+2%	-2%	-5%	-10%	-19%	
		Λ^*	○	+13%	+6%	+2%	+1%	-1%	-2%	-5%	-9%	
r_p	100	r_s^*	○	-18%	-9%	-3%	-2%	+2%	+4%	+9%	+19%	
		τ_t^*	●	+64%	+27%	+10%	+5%	-5%	-9%	-20%	-36%	
		Λ^*	○	+23%	+11%	+4%	+2%	-2%	-4%	-10%	-19%	
γ_0	20 dB	r_s^*	●	+32%	+12%	+4%	+2%	-2%	-4%	-8%	-12%	
		τ_t^*	○	—	—	—	—	—	—	—	—	
		Λ^*	○	+12%	+5%	+2%	+1%	-1%	-2%	-4%	-7%	
P_s	700 mW	r_s^*	○	-24%	-11%	-4%	-2%	+2%	+4%	+9%	+18%	
		τ_t^*	○	-1%	—	—	—	—	—	—	—	
		Λ^*	●	+51%	+19%	+7%	+3%	-3%	-6%	-13%	-22%	
P_{col}	0.04	r_s^*	○	+7%	+3%	+1%	—	—	-1%	-2%	-4%	
		τ_t^*	○	+13%	+6%	+2%	+1%	-1%	-2%	-5%	-9%	
		Λ^*	●	-30%	-14%	-6%	-3%	+3%	+6%	+14%	+27%	
σ_p^2/σ_n^2	10	r_s^*	○	+7%	+2%	+1%	—	—	—	-1%	-2%	
		τ_t^*	○	+16%	+6%	+2%	+1%	-1%	-2%	-4%	-6%	
		Λ^*	●	+32%	-12%	-4%	-2%	+2%	+4%	+9%	+15%	

Legend ○: Not sensitive at all || ○: Slightly sensitive || ○: Mildly sensitive || ●: Significantly sensitive || ●: Very sensitive

reward value decreases with increasing r_p .

r_p has a similar story as ρ_p , having no direct link to likelihood of SSA but impacting the P_{np} probability for SFT completion. Hence, as a response to changes in r_p , τ_t^* is significantly shifted in the opposite direction while r_s^* is mildly moved in the same direction, as disclosed in rows 13-15 of Table V. In fact, τ_t^* is most sensitive to r_p out of all the 9 parameters in scrutiny.

6) *Sensitivity to γ_0 :* Optimal Λ^* is slightly and r_s^* is significantly sensitive to changes in γ_0 , while τ_t^* is not impacted at all. When γ_0 is increased, all else being equal (incl. base value (r_s^*, τ_t^*)), both the achievable rate R and $E\{E_{sft}\}$ increase, as seen in Table IV.

γ_0 has no direct link to SSA or SFT probabilities, yet mainly impacts the consumed energy during attempted transmissions, $E_t = (q_1 r_s^\kappa + q_2) \tau_t$. γ_0 is a linear multiplier term within q_1 . As γ_0 is changed, to arrive at the new optimal Λ^* , system prefers to adjust r_s^* in the opposite direction of the change of γ_0 , rather than τ_t^* . This is driven by the fact that r_s has an exponent $\kappa = 2.5$ in the E_t equation, whereas τ_t is a linear multiplier. Hence, r_s^* is significantly sensitive to and negatively correlated with γ_0 , while τ_t^* is uncorrelated, as shown in rows 16-18 of Table V.

7) *Sensitivity to P_s :* Optimal Λ^* is very sensitive to power consumption during spectrum sensing P_s . When P_s is increased, all else being equal, only $E\{E_{sft}\}$ increases, while no impact is observed on other terms of the Λ^* expression

from (21), as seen in Table IV.

All three possible scenario sets A , B and C contain the term $2E_s = 2P_s \tau_s$ in their energy consumption in each slot. To that end, $2E_s$ is sort of a fixed cost in $E\{E_{sft}\}$ which is consumed until SFT. To that end, when P_s is increased, the system seeks to arrive at the new optimal Λ^* via increasing r_s^* . This increase in r_s^* is driven by the fact that system would like to achieve more of either $\tau_t R$ or $E\{W\}$ as fixed cost in the energy component $E\{E_{sft}\}$ becomes even more important. Raising $\tau_t R$ via increasing τ_t^* is not very feasible, as this increases the likelihood of failed transmissions without SFT, thus increasing $E\{\tau_{sft}\}$ and $E\{E_{sft}\}$. In contrast, r_s^* is linked to SFT probability through the S term in $P_{np} = e^{-\rho_p S(1-e^{-\tau_t \beta})}$, which is a slowly increasing function of r_s . Hence, r_s^* shifts significantly in the same direction as γ_0 , whereas τ_t^* remains intact, as shown in rows 19-21 of Table V.

8) *Sensitivity to P_{col} :* Optimal Λ^* is significantly sensitive to the maximum SU-PU collision probability that a PU can tolerate P_{col} . When P_{col} is increased, the constraint on maximum SU-PU collision probability is relaxed. Consequently, all else being equal (incl. base value (r_s^*, τ_t^*)), both $E\{\tau_{sft}\}$ and $E\{E_{sft}\}$ decrease as seen in Table IV, increasing Λ as a consequence.

We have seen in Fig. 5(a) that as P_{col} decreases, required τ_s significantly increases. Consequently, this increases not only the fixed cost component of energy consumption of amount $2E_s$ but also the time consumed for spectrum sensing τ_s , in

each slot. To that end, as P_{col} decreases, to arrive at the new optimal Λ^* , the system shifts both r_s^* and τ_t^* in the reverse direction. r_s^* is slightly and τ_t^* is mildly sensitive to changes in P_{col} , as shown in rows 22-24 of Table V.

9) *Sensitivity to σ_p^2/σ_n^2 :* Optimal Λ^* is significantly sensitive to PU signal variance as a ratio to noise variance σ_p^2/σ_n^2 . When σ_p^2/σ_n^2 is increased, all else being equal (incl. base value (r_s^*, τ_t^*)), both $E\{\tau_{sft}\}$ and $E\{E_{sft}\}$ decrease as shown in Table IV, raising Λ as a result.

Assuming σ_n^2 fixed, increasing σ_p^2 for a given τ_s decreases the false alarm probability P_{fa} in (1) and the mis-detection probability P_{md} in (4). Hence, to achieve a fixed target $P_{fa} = P_{md}$, τ_s can be reduced when σ_p^2/σ_n^2 is increased. This curtails not only the $2E_s$ amount of energy consumption but also the time for spectrum sensing τ_s , in each slot. Hence, r_s^* and τ_t^* are negatively correlated with σ_p^2/σ_n^2 , with τ_t^* being more sensitive (in rows 25-27 of Table V).

E. Sensitivity of r_s^* , τ_t^* and reward to κ , β and α

As revealed in Table V, Λ is most sensitive to changes in κ , β and α . Hence, we investigate the combined effect of changes in κ , β and α to $(r_s^*, \tau_t^*, \Lambda^*)$ in Fig. 8. In this representation, each row stands for a fixed α value ($\alpha = 10$, $\alpha = 20$ and $\alpha = 30$ for first, second and third rows, respectively) and each column stands for a fixed β value ($\beta = 10$, $\beta = 20$ and $\beta = 30$ for first, second and third columns, respectively). Additionally, each sub-figure displays 15 data points, each corresponding to a case on $\kappa = 2$ to $\kappa = 3.4$ with 0.1 steps. We also fix the PU guardring radius as $r_p = 100$ m, with the condition that $r_s \leq r_p$, which is the usual case for CRSNs.

Accordingly, each sub-figure starts the data points with $\kappa = 2.0$ scenario, which yields $r_s^* = 100$ m in all 9 cases. Again in all cases, r_s^* stays at 100 m for 3-4 data points corresponding to $\kappa = 2.0, 2.1, 2.2, 2.3$ scenarios, while τ_t^* is decreased. After $\kappa = 2.4$ or $\kappa = 2.5$ depending on the case, r_s^* is consistently reduced and τ_t^* is consistently boosted toward $\kappa = 3.4$ scenario.

As previously revealed in Section V-D1, r_s^* moves in a very sensitive manner in the reverse direction of the change in κ , whereas τ_t^* moves significantly in the same direction as κ . Hence, in each sub-figure, we see an increase in r_s^* until 100 m, as κ is decreased from 3.4 to 2.3-2.4. After that point, further decrease in κ cannot trigger any more r_s^* increase as it is capped by $r_p = 100$ m. Therefore, we observe an increase in τ_t^* as we further reduce κ from 2.3-2.4 levels to 2.0, despite they are being positively correlated under normal circumstances. Key highlights on sensitivities of $(r_s^*, \tau_t^*, \Lambda^*)$ on κ , β and α are as follows:

- All three are most sensitive to κ . r_s^* and Λ^* move in reverse direction of κ , whereas τ_t^* follows κ with the exception of when r_s^* is capped to 100 m.
- Increasing β decreases τ_t^* significantly irrespective of κ value (except when r_s^* is capped to 100 m). Assuming $\alpha = 10$, increasing β from 10 to 20 and from 10 to 30 reduces τ_t^* by $\sim 33\%$ and $\sim 50\%$, respectively. Boosting α smoothens this decrease. As an example, when $\alpha = 30$, τ_t^* decreases by $\sim 29\%$ and $\sim 45\%$ for the same increases in β .

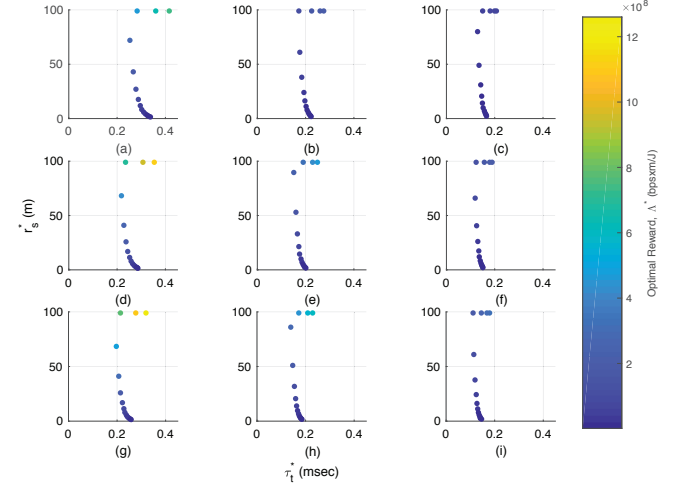


Fig. 8: Optimal $(r_s^*, \tau_t^*, \Lambda^*)$ with respect to (a) $\alpha = 10$, $\beta = 10$; (b) $\alpha = 10$, $\beta = 20$; (c) $\alpha = 10$, $\beta = 30$; (d) $\alpha = 20$, $\beta = 10$; (e) $\alpha = 20$, $\beta = 20$; (f) $\alpha = 20$, $\beta = 30$; (g) $\alpha = 30$, $\beta = 10$; (h) $\alpha = 30$, $\beta = 20$; (i) $\alpha = 30$, $\beta = 30$, when κ changes from 2.0 to 3.4 with 0.1 steps, and PU guardring radius set as $r_p = 100$ m,

- Increasing α decreases τ_t^* significantly irrespective of κ value. If $\beta = 10$, increasing α from 10 to 20 and from 10 to 30 reduces τ_t^* by 15% and 24%, respectively. Boosting β smoothens this decrease. When $\beta = 30$, τ_t^* decreases by 9% and 13% for the same increases in α .

VI. CONCLUSIONS

In this paper, we formulate the problem of finding energy-efficient transmission range r_s and transmission duration τ_t for CRSN deployment that would minimize the energy consumed per goodput per meter toward the sink in a greedy forwarding scenario. For that purpose, we first characterize the transmissions in CRSN under DSA; deriving the probability of successful frame transmission at each attempt between one-hop neighbor CRSN nodes. Leveraging expected hop progress toward the sink and expected hop distance concepts, we reveal the expected time and energy consumption until successful frame transmission under different spectrum utilization scenario probabilities. Finally, we formulate our optimization problem as a reward function Λ that represents goodput times expected hop progress toward the sink per Joule. Our findings reveal that

- Path loss exponent κ is by far the parameter that r_s^* and Λ^* are most sensitive to,
- Apart from κ , Λ^* is also very sensitive to PU birth rate β , PU death rate α , SU power consumption during spectrum sensing P_s , maximum SU-PU collision probability that a PU can tolerate P_{col} and PU signal variance σ_p^2 ,
- Apart from κ , r_s^* is also very sensitive to reference SNR needed at SU receiver for demodulation γ_0 and SU power consumption during spectrum sensing P_s ,
- τ_t^* is impacted by κ , PU guardring radius r_p , PU death rate α and PU node density ρ_p .

These relations provide valuable insights for detailed CRSN design prior to deployment. As future work, we will investigate

effects of noise variance in channel sensing and fading channel on energy-efficient transmission range and duration, which require further analysis on bit error rates and algorithm designs on the spectrum sensing.

REFERENCES

- [1] O. B. Akan, O. B. Karli and O. Ergul, "Cognitive Radio Sensor Networks," *IEEE Network*, vol. 23, no. 4, pp. 34-40, 2009.
- [2] S. R. Gandham, M. Dawande, R. Prakash and S. Venkatesan, "Energy Efficient Schemes for Wireless Sensor Networks with Multiple Mobile Base Stations," in *Proc. IEEE GLOBECOM*, 2003, pp. 377-381.
- [3] C. Bettstetter, "On the Minimum Node Degree and Connectivity of a Wireless Multihop Network," in *Proc. ACM MobiHoc*, 2002, pp. 80-91.
- [4] S. De, "On Hop Count and Euclidean Distance in Greedy Forwarding in Wireless Ad Hoc Networks," *IEEE Communications Letters*, vol. 9, no. 11, pp. 1000-1002, 2005.
- [5] J. Deng, Y. S. Han, P. N. Chen and P. K. Varshney, "Optimal Transmission Range for Wireless Ad Hoc Networks Based on Energy Efficiency," *IEEE Transactions on Communications*, vol. 55, no. 7, pp. 1439-1439, 2007.
- [6] P. Chen, B. O'Dea and E. Callaway, "Energy Efficient System Design with Optimum Transmission Range for Wireless Ad Hoc Networks," in *Proc. IEEE ICC*, 2002, pp. 945-952.
- [7] H. Zhang, Z. Zhang, X. Chen and R. Yin, "Energy Efficient Joint Source and Channel Sensing in Cognitive Radio Sensor Networks," in *Proc. IEEE ICC*, 2011, pp. 1-6.
- [8] M. Monemian, M. Mahdavi and M. J. Omidi, "Improving the lifetime of multichannel cognitive radio sensor networks via new spectrum sensing method," *Wiley Transactions on Emerging Technologies*, vol. 30, no. 5, pp. 1-21, 2019.
- [9] H. Kaschel *et al.*, "Energy-Efficient Cooperative Spectrum Sensing Based on Stochastic Programming in Dynamic Cognitive Radio Sensor Networks," *IEEE Access*, vol. 9, pp. 720-732, 2021.
- [10] J. A. Han, W. S. Jeon and D. G. Jeong, "Energy-Efficient Channel Management Scheme for Cognitive Radio Sensor Networks," *IEEE Transactions on Vehicular Technology*, vol. 60, no. 4, pp. 1905-1910, 2011.
- [11] P. M. Rodriguez *et al.*, "Spectrum handoff strategy for cognitive radio-based MAC for real-time industrial wireless sensor and actuator networks," *Computer Networks (Elsevier)*, vol. 152, pp. 186-198, Apr. 2019.
- [12] M. Ozger, F. Alagoz and O. B. Akan, "Clustering in Multi-Channel Cognitive Radio Ad Hoc and Sensor Networks," *IEEE Communications Magazine*, vol. 56, no. 4, pp. 156-162, 2018.
- [13] M. C. Oto and O. B. Akan, "Energy-efficient Packet Size Optimization for Cognitive Radio Networks," *IEEE Transactions on Wireless Communications*, vol. 11, no. 4, pp. 1544-1553, 2012.
- [14] S. Gao, L. Qian, D. R. Vaman and Q. Qu, "Energy Efficient Adaptive Modulation in Wireless Cognitive Radio Sensor Networks," in *Proc. IEEE ICC*, 2007, pp. 3980-3986.
- [15] F. A. Awin, Y. M. Alginahi, E. Abdel-Raheem and K. Tepe, "Technical Issues on Cognitive Radio-Based Internet of Things Systems: A Survey," *IEEE Access*, vol. 7, pp. 97887-97908, 2019.
- [16] M. H. Rehmani, S. Lohier and A. Rachedi, "Channel Bonding in Cognitive Radio Wireless Sensor Networks," in *Proc. International Conference on Selected Topics in Mobile and Wireless Networking*, 2012, pp. 72-76.
- [17] M. Zheng *et al.*, "A Short Preamble Cognitive MAC Protocol in Cognitive Radio Sensor Networks," *IEEE Sensor Journal*, vol. 19, no. 15, pp. 6530-6538, 2019.
- [18] Y. Ge, S. Wang and J. Ma, "Optimization on TEEN routing protocol in cognitive wireless sensor network," *EURASIP Journal on Wireless Communications and Networking*, vol. 27, pp. 1-9, 2018.
- [19] M. M. Hassani and R. Berangi, "Impact of Secondary User Block on the TCP Throughput in Cognitive Radio Sensor Networks," *Springer Wireless Personal Communications*, vol. 109, pp. 1-18, 2019.
- [20] Z. Shang, T. Zhang, G. Hu, Y. Cai and W. Yang, "Secure Transmission for NOMA-Based Cognitive Radio Networks With Imperfect CSI," *IEEE Communications Letters*, vol. 25, no. 8, pp. 2517-2521, 2021.
- [21] Z. Shang, T. Zhang, Y. Cai, Y. Liu and W. Yang, "Secure Spectrum-Sharing Wiretap Networks With Full-Duplex Relaying," *IEEE Access*, vol. 7, pp. 181610-25, 2019.
- [22] T. He, K. -W. Chin, S. Soh and Z. Zhang, "A Novel Distributed Resource Allocation Scheme for Wireless Powered Cognitive Radio Internet of Things Networks," *IEEE Internet of Things Journal*, vol. 8, no. 20, pp. 1-15, 2021.
- [23] M. Ozger and O. B. Akan, "On the Utilization of Spectrum Opportunity in Cognitive Radio Networks," *IEEE Communications Letters*, vol. 20, no. 1, pp. 157-160, 2016.
- [24] A. O. Bicen, E. B. Pehlivanoglu, S. Galmes and O. B. Akan, "Dedicated Radio Utilization for Spectrum Handoff and Efficiency in Cognitive Radio Networks," *IEEE Transactions on Wireless Communications*, vol. 14, no. 9, pp. 5251-5259, 2015.
- [25] B. Karp and H.T. Kung, "GPSR: Greedy Perimeter Stateless Routing for Wireless Networks," in *Proc. ACM MOBICOM*, 2000, pp. 243-254.
- [26] J. Li, J. Jannotti, D. S. J. De Couto, D. R. Karger and R. Morris, "A Scalable Location Service for Geographical Ad Hoc Routing," in *Proc. ACM MOBICOM*, 2000, pp. 120-130.
- [27] W. Y. Lee and I. F. Akyildiz, "Optimal Spectrum Sensing Framework for Cognitive Radio Networks," *IEEE Transactions on Wireless Communications*, vol. 7, no. 10, pp. 3845-3857, 2008.
- [28] R. Zhang, J. M. Gorce, R. Dong and K. Jaffres-Runser, "Energy efficiency of Opportunistic Routing with Unreliable Links," in *Proc. IEEE WCNC*, 2009, pp. 1-6.
- [29] IEEE Standard for Local and Metropolitan Area Networks—Part 15.4: "Low-Rate Wireless Personal Area Networks (LR-WPANs)," *IEEE Std 802.15.4-2011*, pp. 1-314, 2011.
- [30] R. Zhang and J. M. Gorce, "Optimal Transmission Range for Minimum Energy Consumption in Wireless Sensor Networks," in *Proc. IEEE WCNC*, 2008, pp. 757-762.
- [31] J. M. Gorce, R. Zhang and H. Parvary, "Impact of Radio Unreliability on the Connectivity of Wireless Sensor Networks," *EURASIP Journal on Wireless Communications and Networking*, vol. 2007, 2007.